Journal of New Materials for Electrochemical Systems 16, 273-278 (2013)

Synthesis of Medium-temperature Protonic Conductor $CsHSO_4$-Al_2O_3

L.B. Yang[1], W.S. Ning[2], X.D. Wang[1], W. Liu[1], H.Y. Shen[1,*], Y.X. Huang[1] and K.Y. Shu[1]

[1]College of Materials Science and Engineering, China Jiliang University, Hangzhou 310018, China
[2]State Key Laboratory Breeding Base of Green Chemistry-Synthesis Technology,
Zhejiang University of Technology, Hangzhou 310032, China.

Received: July 02, 2013, Accepted: July 15, 2013, Available online: September 18, 2013

Abstract: *In this study, different methods are used to synthesize novel medium-temperature protonic conductors from $CsHSO_4$ and mesoporous Al_2O_3. X-ray diffraction, scanning electron microscopy, thermogravimetric analysis and differential scanning calorimetry, and nitrogen adsorption-desorption isotherms are performed to investigate the structures and properties of $CsHSO_4$-Al_2O_3 conductors. Results show that the proton conductivities of the prepared $CsHSO_4$-Al_2O_3 conductors increase as temperature increases from 100 °C to 200 °C. The optimum method involves mixing the equimolar $CsHSO_4$ and Al_2O_3 with 5 ml ethanol and subsequently ball milling at a rotating speed of 200 rpm for 2 h. The highest proton conductivity obtained in this study is 1.06×10^{-6} $S\cdot cm^{-1}$ at 200 °C.*

Keywords: Composite; Proton conductivity; Proton carrier

1. INTRODUCTION

Solid proton-conducting materials have attracted much attention for their potential applications in clean energy fields, such as fuel cells, electrolytic cells, and chemical sensors [1–3]. Among these applications, Nafion-based polymer electrolyte membranes are one of the most successfully used within a temperature range between 25 °C and 90 °C [4]. However, proton conductivity of Nafion drops seriously above 100 °C. In addition, the catalyst is more easily poisoned by carbon monoxide at a temperature below 100 °C and the methanol permeability in direct methanol fuel cells is high [5]. Novel proton-conducting materials that can be used at a medium temperature range of 100 °C to 200 °C may developed to compensate these shortages and lots of novel composite material systems have been wildly studied [6-7].

From those systems, stable inorganic porous materials with high conductivity are considered a good choice. However, only a few studies have focused on these materials [8-9]. Inorganic porous oxides, such as SiO_2 and Al_2O_3, exhibit high proton conductivity, particularly above 100 °C, because of their mesoporous structures that allow water adsorption. In addition, $CsHSO_4$ (CHS), a medium-temperature proton-conducting material, can be used as a solid electrolyte for fuel cells [10]. CHS undergoes a superprotonic phase transition at approximately 140 °C that is accompanied by a significant increase in proton conductivity from 10^{-6} $S\cdot cm^{-1}$ to 10^{-2} $S\cdot cm^{-1}$ [11]. However, water solubility and mechanical fragility of CHS limit its use as an electrolyte.

In our previous study [12-16], we synthesized a mesoporous alumina with high proton conductivity below 100 °C. In order to improve the proton conductivity of mesoporous alumina in the medium temperature range, novel protonic conductors with high conductivity from 100 °C to 200 °C were prepared by composing CHS with mesoporous alumina. The pore structure, proton conductivity, and conductivity mechanism were changed using different preparation methods.

2. EXPERIMENT

Polycrystalline CHS powders were obtained by subjecting the aqueous solutions of equimolar H_2SO_4 (purity > 99%; ACROS) and Cs_2SO_4 to isothermal evaporation at 80 °C for 24 h. X-ray diffraction (XRD) revealed that the as-grown crystals were in phase III (Fig. 1), indicating that the polycrystalline CHS was pure and exhibited a low-temperature phase.

Mesoporous Al_2O_3 was synthesized using the sol-gel method [17]. CHS powders were composited with mesoporous Al_2O_3 based on four different methods and produced four samples (A, B, C, and D). Equimolar ratios of polycrystalline CHS powders and

*To whom correspondence should be addressed: Email: shenhangyan@cjlu.edu.cn
Phone: 86-571-86835745, Fax.: 86-571-86835740

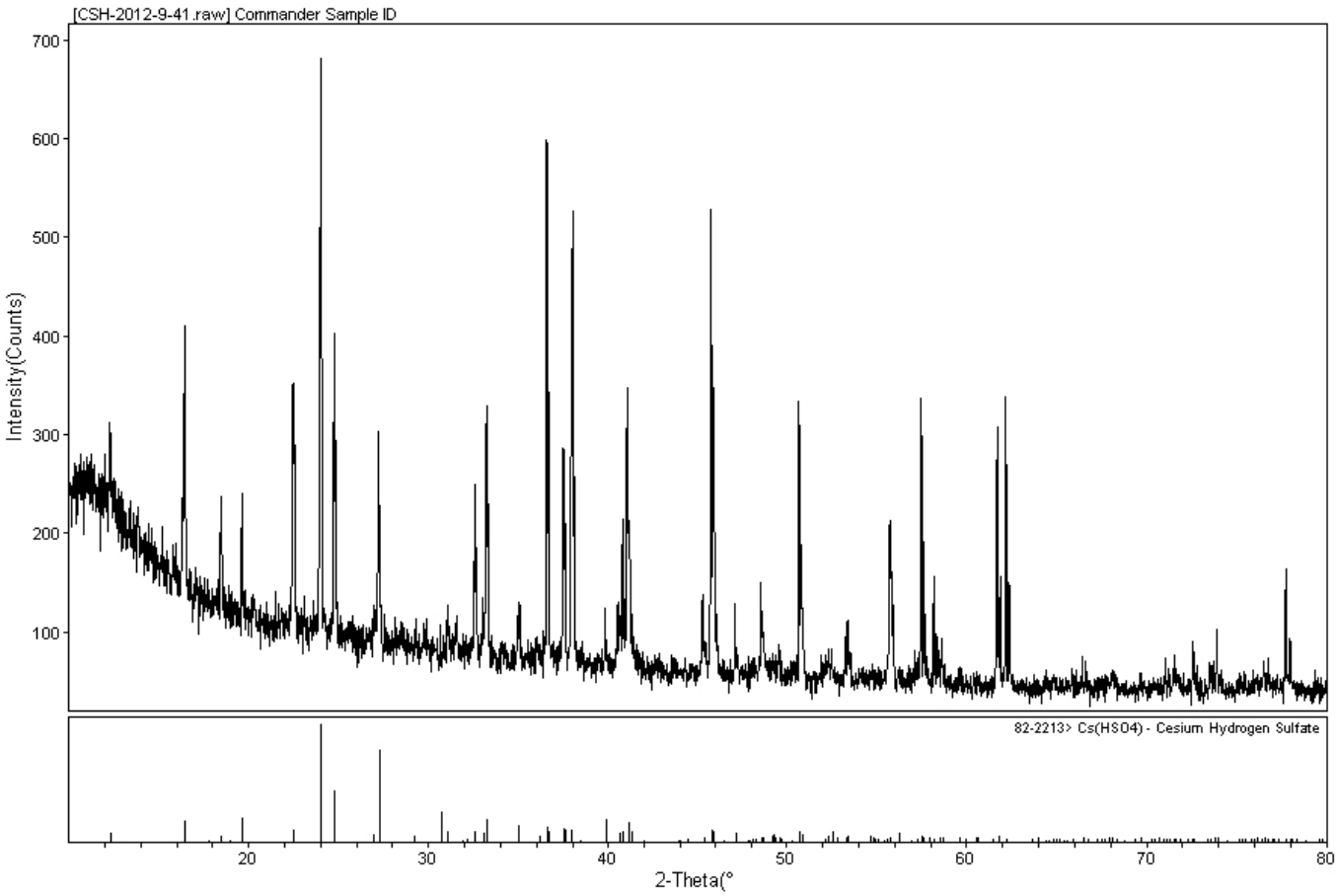

Figure 1. XRD pattern of CHS powder.

mesoporous Al_2O_3 powders were controlled for synthesis. Sample A was prepared by mixing CHS and Al_2O_3 powders, which were subsequently subjected to isothermal treatment at 250 °C for 2 h. Sample B was prepared by manually grinding CHS and Al_2O_3 with an agate mortar for 2 h. Sample C was obtained by ball milling at a rotating speed of 200 rpm for 2 h. Sample D was prepared by mixing CHS and Al_2O_3 with 5 ml ethanol; the resulting mixture was then ball milled at a rotating speed of 200 rpm for 2 h.

The crystal structure of the conductor powders performed by XRD using an X'Pert Pro Holland diffractometer (CuK_α, 40 kV, 30 mA) at a 2θ range of 10° to 80°.

A scanning electron microscope (SEM, HITACHI S-4700) was used to analyze the surface morphology. The samples were vapor deposited with gold before analysis. A JEOL JSM-5610LV SEM equipped with an energy dispersive spectroscope (EDS) was used to identify the elemental distribution.

Thermogravimetric analysis and differential scanning calorimetry (TG-DSC) performed using a METTLER TOLEDO STAR instrument at a heating rate of 2 °C/min from 25 °C to 300 °C.

The average pore size, pore volume, and specific surface areas (S_{BET}) were obtained by N_2 adsorption-desorption isotherms with a TriStar II 3020 instrument.

The proton conductivity was determined by AC impedance spec-

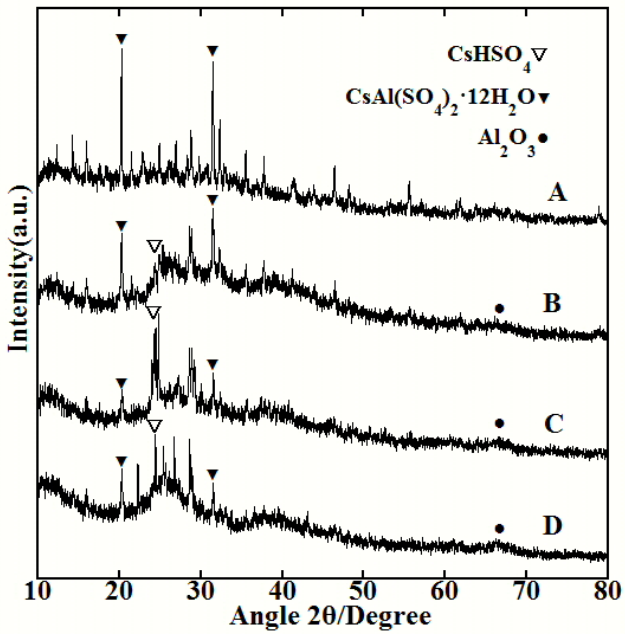

Figure 2. XRD patterns of all different CHS-Al_2O_3 conductors.

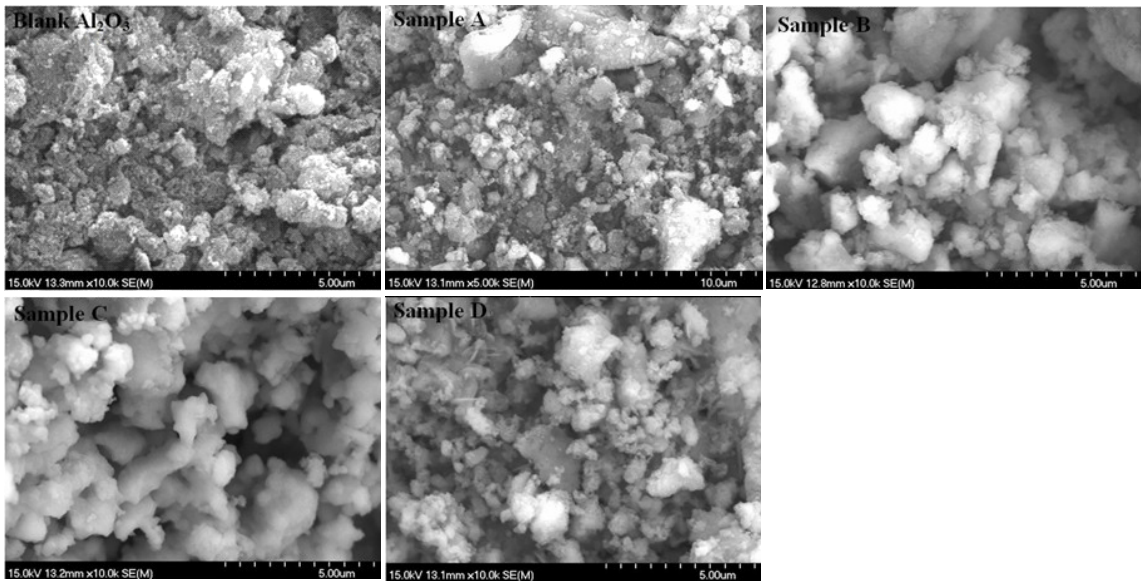

Figure 3. Images of mesoporous Al_2O_3 and different CHS-Al_2O_3 conductors.

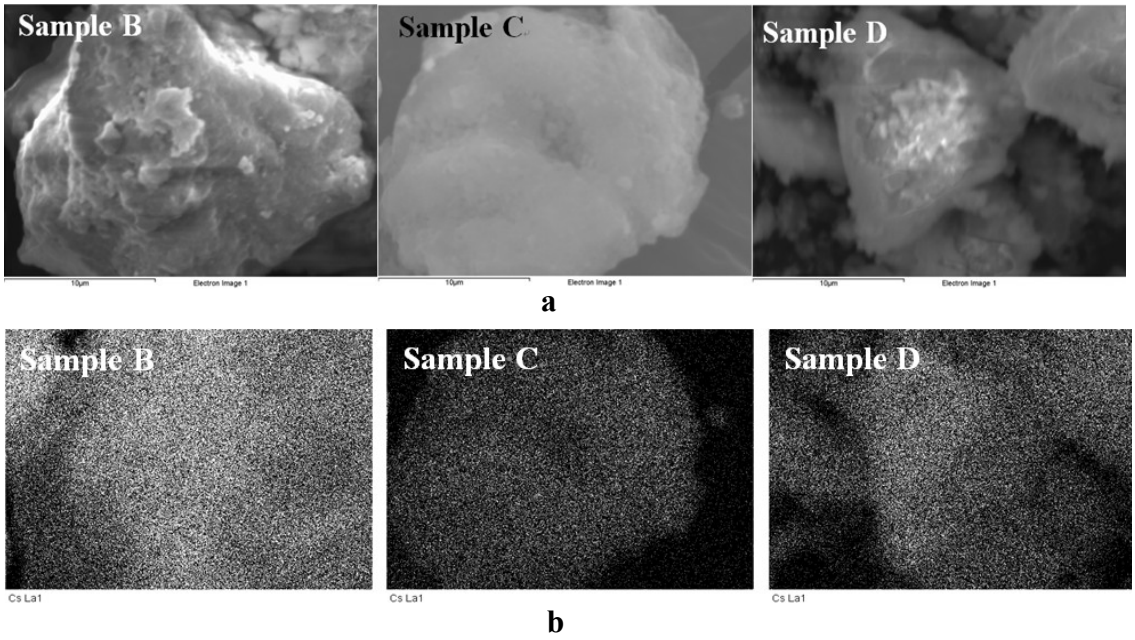

Figure 4. Cs mapping results. (a) SEM pictures of sample B, C and D. (b) Cs distribution of sample B, C and D.

troscopy (Agilent 4294A impedance spectroscope) at a frequency range of 40 Hz to 30 MHz. Before measurement, the samples were pressed into tablets with cold isostatic press method at 200 MPa. Platinum electrodes were sputtered onto both sides of the tablets by using a vacuum magnetron sputter. The samples were then placed between two stainless steel electrodes and transferred in a draught drying chamber to determine the proton conductivity. Impedance was determined stepwise from 100 °C to 200 °C.

3. RESULTS AND DISCUSSION

3.1. Structural analysis

Fig. 2 shows the XRD patterns of different CHS-Al_2O_3 conductors. The peaks at $2\theta = 21.2°$ and 32.4° correspond to the reflections of $CsAl(SO_4)_2 \cdot 12H_2O$. The XRD curves indicate that several $CsAl(SO_4)_2 \cdot 12H_2O$ crystals are found in sample A, but only a few are found in samples B, C, and D. The peaks at 25.5° and 67.1° belong to CHS and Al_2O_3, respectively, which are found in the curves of samples B, C, and D.

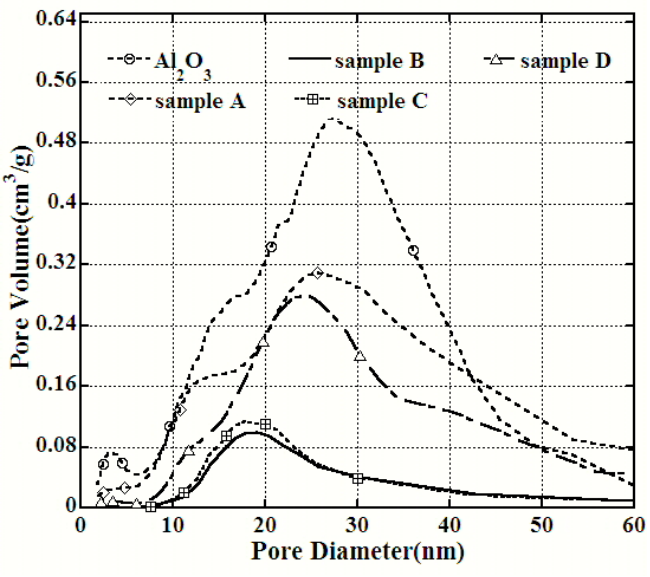

Figure 5. Pore size distribution determined from the desorption branch of the N_2 desorption isotherm.

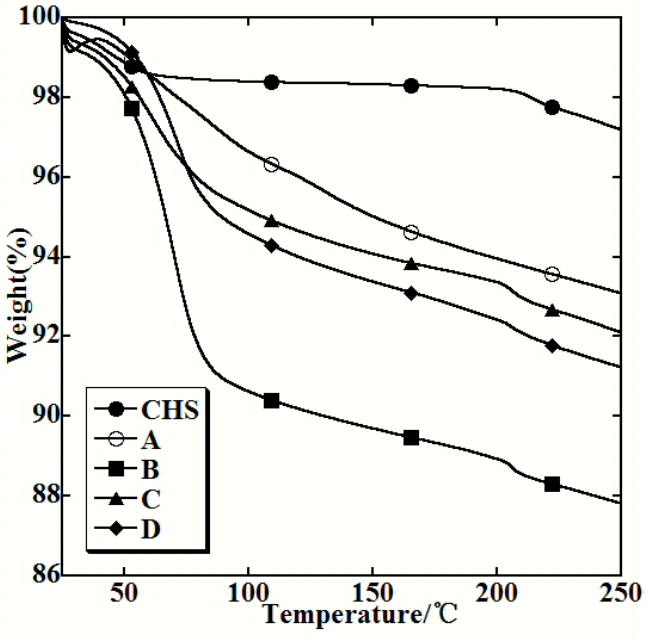

Figure 6. TG results of pure CHS and different CHS-Al_2O_3 conductors.

3.2. Morphology

The SEM images of the CHS-Al_2O_3 conductors are shown in Fig. 3. The morphology of sample A is similar to that of the mesoporous Al_2O_3. However, the water solubility of CHS caused the particles of the other samples to aggregate. Fig. 4 shows the Cs EDS mapping results of samples B, C, and D. In particular, Cs is evenly distributed in samples C and D However unevenly distributed in sample B (Fig. 4), indicating that mechanical milling is more efficient than manual grinding.

3.3. Pore structure

S_{BET} of the samples are shown in Table 1. In particular, S_{BET} of the CHS-Al_2O_3 samples decreased after compositing, particularly for samples B and C. S_{BET} was approximately 30 times lower than that of the pure mesoporous Al_2O_3. Fig. 5 shows the pore size distribution of the samples. In particular, the pore size was distributed within the range of 10 nm to 30 nm. The pore size and pore volume were decreased for the CHS-Al_2O_3 samples, particularly for samples B and C, because the CHS particles probably filled the pores of Al_2O_3 and some mesopores were destroyed by mechanical strength, thereby decreasing the pore volume. Ethanol, as an auxiliary agent, can also decrease the mechanical strength of ball milling. As a result, S_{BET} of sample D was approximately three times higher than that of samples B and C.

3.4. TG-DSC analysis

The results of TG-DSC analysis are shown in Figs. 6 and 7. The TG curves of the samples declined abruptly at approximately 75 °C because the physically adsorbed water evaporated [15]. In addition, the loss of the water molecule contained in the meso porous of the samples lasted from 100 °C – 200 °C, leading to the slow decline of the TG curve within the temperature range. The DSC results are consistent with the TG curves. All of the samples have an endother-

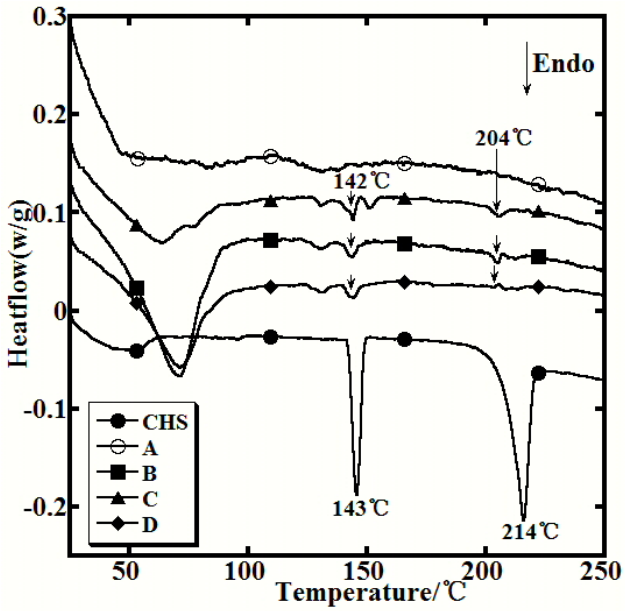

Figure 7. DSC results of pure CHS and different CHS-Al_2O_3 conductors.

Table 1. Specific surface areas (SBET) of all samples.

Sample	Al_2O_3	A	B	C	D
$S_{BET}(m^2/g)$ [a]	303.2532	50.9755	7.2496	8.4130	27.6085

[a] Specific surface area of the samples.

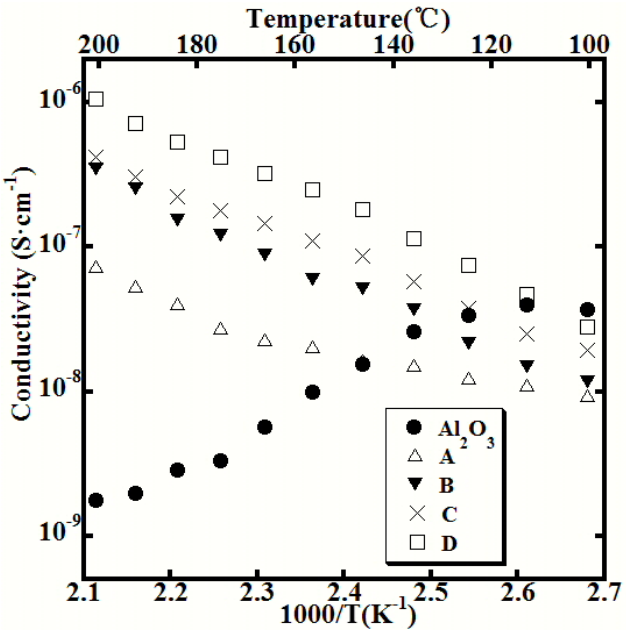

Figure 8. Proton conductivity of mesoporous Al_2O_3 and CHS-Al_2O_3 conductors.

mic peak at approximately 75 °C. Furthermore, samples B, C, and D exhibited two normal endothermic peaks at 142 °C and 204 °C, which correspond to the superprotonic phase transition and the melting point of CHS [18], respectively. These peaks are not found in the TG curve of sample A. The TG-DSC results are also consistent with the XRD curves, indicating that the crystalline CHS is also found in samples B, C, and D. In sample A, CHS reacted with Al_2O_3 to form $CsAl(SO_4)_2 \cdot 12H_2O$.

3.5. Proton conductivity

The temperature dependence of the conductivities of mesoporous Al_2O_3 and CHS-Al_2O_3 are shown in Fig. 8. In particular, the conductivity of the mesoporous Al_2O_3 decreased as temperature increased from 100 °C to 200 °C, whereas the conductivity of the CHS-Al_2O_3 samples increased. Conductivity also changed depending on the synthesis method used. For instance, sample D had the highest conductivity, but sample A exhibited the lowest conductivity. At 200 °C, the conductivity of sample D (1.06×10^{-6} $S\cdot cm^{-1}$) was higher than that of sample A (7.31×10^{-8} $S\cdot cm^{-1}$) and mesoporous Al_2O_3 (1.78×10^{-9} $S\cdot cm^{-1}$). The proton-conducting activation energies of the CHS-Al_2O_3 conductors are listed in Table 2.

The proton carriers in mesoporous Al_2O_3 are mainly water molecules that are absorbed in the mesopores [12, 13]. The amount of water molecules decreased as the temperature increased from 100 °C to 200 °C, thereby decreasing the proton conductivity. The loss of the water molecule from 100 °C – 200 °C in the mesoporous A-D still has the effect on the proton conductivity. On the other hand, the proton-conducting activation energy of sample A was 28.7 kJ/mol, which is within the range of activation energies for Grotthuss mechanism (14 kJ/mol to 40 kJ/mol) [19]. In this mechanism, the proton is dissociated from the hydroxyl groups and hopped among the water molecules. In this study, the crystal water in sample A was dissociated from $CsAl(SO_4)_2 \cdot 12H_2O$ and acted as the proton carrier, which increased the proton conductivity within the temperature range of 100 °C to 200 °C. The activation energies were 49.59, 44.96, and 51.37 kJ/mol for samples B, C, and D, respectively. In general, the proton transmission medium should be different from the Grotthuss mechanism. CHS was probably present as another proton carrier in these samples. However, no steep increase of conductivity below 150°C was observed because of the low content of CHS in the sample. Higher S_{BET} of sample D (27.6085 m^2/g) than samples B (7.2496 m^2/g) and C (8.4130 m^2/g) may yield higher amounts of active sites that were absorbed on the pore surface, thereby producing the highest proton conductivity.

Table 2. The proton conducting activation energies of CHS-Al_2O_3 conductors.

Sample	A	B	C	D
Ea($kJ\cdot mol^{-1}$) [a]	28.70	49.59	44.96	51.37

[a] The proton conducting activation energy value of samples.

4. CONCLUSIONS

The proton conductors with high conductivities within the medium temperature range were synthesized by compositing CHS and Al_2O_3 based on different methods. $CsAl(SO_4)_2 \cdot 12H_2O$, which was formed in sample A, functioned as the proton carrier that affected the proton conductivity within the medium temperature range. CHS was present in samples B, C, and D, thereby affecting the proton conductivities in these samples within the medium temperature range. The results demonstrated that the most efficient sample obtained using different methods was sample D, which retained CHS on the Al_2O_3 surface and achieved a higher S_{BET} than samples B and C, thereby producing a higher conductivity within the medium temperature range.

5. ACKNOWLEDGEMENTS

This work is supported financially by the National Science Foundation of China (No. 51072189 and 21003111) and Xinmiao Talents Program of Zhejiang province (No. 2011R409040).

REFERENCES

[1] Y. Abe, M. Hayashi, T. Iwamoto, H. Sumi, L.L. Hench, J. Non-Cryst. Solids, 351, 2138 (2005).
[2] H. Li, M. Nogami, Adv. Mater., 14, 912 (2002).
[3] X.L. Chen, C.S. Wang, E.A. Payzant, C.R. Xia, D. Chu. J. Electrochem. Soc., 155, 1264 (2008).
[4]C. Yang, S. Srinivasan, A.B. Bocarsly, S. Tulyani, J.B. Benziger, J. Membr. Sci., 237, 145 (2004).
[5] H.Y. Chang, C.W. Lin, J. Membr. Sci., 218, 295 (2003).
[6] O. Savadogo, J. New Mater. Electrochem. Syst., 1, 47 (1998).
[7] O. Savadogo, J. Power Sources, 127, 135 (2004).
[8] M. Nogami, Y. Usui, T. Kasuga, Fuel Cells, 3, 181 (2001).
[9] R. Marschall, I. Bannat, J. Caro, M. Wark, Microporous Mesoporous Mater., 99, 190 (2007).
[10]S.M. Haile, D.A. Boysen, C.R.I. Chisholm, R.B. Merle, Nature, 410, 910 (2001).

[11]S.Q. Wang, J. Otomo, M. Ogura, Q. Wen, H. Nagamoto, H. Takahashi, Solid State Ionics, 176, 755 (2005).
[12]H.Y. Shen, H. Maekawa, J. Kawamura, T. Yamamura, Solid State Ionics, 177, 2403 (2006).
[13]H.Y. Shen, H. Maekawa, J. Kawamura, Y. Matsumoto, T. Yamamura, Y. Kawakita, K. Shibata, M. Kawai, Solid State Ionics, 179, 1133 (2008).
[14]H.Y. Shen, H. Maekawa, L. Wang, B. Guo, K.Y. Shu, Electrochem. Solid-State Lett., 12, B18 (2009).
[15]H.Y. Shen, B. Guo, H. Maekawa, J.Y. Guo, K.Y. Shu, Solid State Ionics, 192, 105 (2011).
[16]X.D. Wang, L.B. Yang, J.B. Liu, Y.X. Huang, H.Y. Shen, K.Y. Shu, Adv. Mater. Res., 472, 2819 (2012).
[17]H. Maekawa, R. Tanaka, T. Sato, Y. Fujimaki, T. Yamamura, Solid State Ionics, 175, 281 (2004).
[18]E. Ortiz, R.A. Vargas, B-E. Mellander, J. Phys. Condens. Matter, 18, 9561 (2006).
[19]M.T. Colomer, M.A. Anderson. J. Non-Cryst. Solids, 290, 93 (2001).